Published in final edited form as:

Structure. 2016 August 2; 24(8): 1248–1256. doi:10.1016/j.str.2016.05.016.

Model of the ankyrin and SOCS box protein, ASB9, E3 ligase reveals a mechanism for dynamic ubiquitin transfer

Jamie M. Schiffer[1], **Robert D. Malmstrom**[1,2], **Jonathan Parnell**[1], **Cesar Ramirez-Sarmiento**[3], **Javiera Reyes**[3], **Rommie E. Amaro**[1,2,*], and **Elizabeth A. Komives**[1,*]

[1] Department of Chemistry and Biochemistry, University of California, San Diego, 9500 Gilman Drive, La Jolla, California 92093-0378, United States.

[2] National Biomedical Computation Resource, University of California, San Diego, 9500 Gilman Drive, La Jolla, California 92093-0608, United States.

[3] Departamento de Biologia, Facultad de Ciencias, Universidad de Chile, Las Palmeras 3425, Casilla 653, Santiago 7800003, Chile

Summary

Cullin-RING E3 Ligases (CRLs) are elongated and bowed protein complexes that transfer ubiquitin over 60 Å to proteins targeted for proteasome degradation. One such CRL contains the ankyrin repeat and SOCS box protein 9 (ASB9), which binds to and partially inhibits creatine kinase (CK). While current models for the ASB9-CK complex contain some known interface residues, the overall structure and precise interface of the ASB9-CK complex remains unknown. Through an integrative modeling approach, we report a third generation model that reveals precisely the interface interactions and also fits the shape of the ASB9-CK complex as determined by SAXS. We constructed an atomic model for the entire CK-targeting CRL to uncover dominant modes of motion that could permit ubiquitin transfer. Remarkably, only the correctly docked CK-containing E3 ligase and not incorrectly docked structures permitted close approach of ubiquitin to the CK substrate.

Graphical Abstract

* Correspondence to: ekomives@ucsd.edu; ramaro@ucsd.edu.

Author Contributions

J.S., R.D.M., C.S., R.E.A, and E.A.K collaborated in planning of project. J.S. executed majority of experiments and entirety of computational work, performed analysis, and wrote the paper with E.A.K. R.D.M. provided mentorship and in-house scripts, and assisted in building of computational protein systems. J. P. purified protein for SAXS analysis. C.S. and J.R. performed mutagenesis experiments. R.E.A. and E.A.K. were leading investigators and edited paper.

Cullin-RING E3 Ligases (CRLs) are multi-protein complexes which transfer ubiquitin over 60 Å to a protein doomed for degradation. Schiffer et al. construct an atomic model for a CRL that ubiquitinates creatine kinase (CK) and uncover dominant modes of motion that could permit ubiquitin transfer.

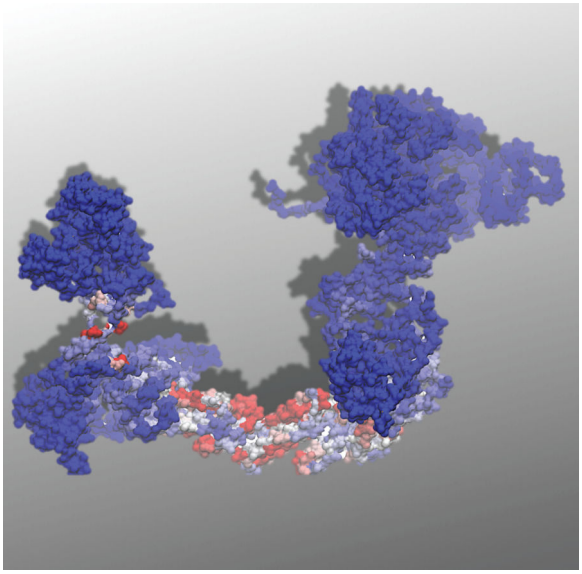

Introduction

Ubiquitin-mediated degradation regulates cellular concentrations of proteins critical to cellular function, including metabolic enzymes and signaling proteins. Cells have evolved to conjugate ubiquitin to a substrate protein by a cascade of three enzymes: E1 ubiquitin-activating enzyme, E2 ubiquitin-conjugating enzyme, and E3 ubiquitin ligase. E3 ligases catalyze the transfer of ubiquitin from E2 enzymes to protein substrates (Deshaies & Joazeiro 2009), and after multiple rounds, the poly-ubiquitination of a protein substrate flags it for destruction by the proteasome (Petroski & Deshaies 2005). Although over 600 human E3 ligases have been identified, only a small percentage of E3 ligase structures have been solved, and even less is known about the conformational dynamics of these multi-protein complexes, despite being ubiquitous and attractive therapeutic targets against tumor malignancies (Deshaies & Joazeiro 2009; Kerscher et al. 2006; Zhao & Sun 2013). The Cullin-RING of E3 ligases (CRLs) are the most abundant types of E3 ligases and form an extended multi-protein complex. Previous models of CRLs show a the distance of over 60 Å between ubiquitin, positioned on the C-terminal end of Cullin protein, and the target protein, positioned at the N-terminal end the Cullin. Thus, substantial conformational changes must be required for ubiquitin transfer (Thomas et al. 2013; Duda et al. 2008).

One such CRL contains the ankyrin repeat and suppressor of cytokine signaling (SOCS) box protein 9 (ASB9), which forms the substrate recognition domain in an Elongin-Cullin-SOCS box-type (ECS-type) E3 ligase. ASB9 interacts directly with the E3 ligase protein substrate, creatine kinase, targeting it for ubiquitin-mediated degradation (Debrincat et al. 2007; Kwon et al. 2010). As one of eighteen members of the ASB family, the largest family of SOCS box containing proteins (Kohroki et al. 2005), ASB9 is composed of an intrinsically disordered N-terminus, an ankyrin repeat domain and the SOCS box domain. While the SOCS box interacts with Elongin B, Elongin C, and Cullin 5 in the E3 ligase complex (Thomas et al. 2013; Muniz et al. 2013), the ankyrin repeat domain and N-terminal disordered segment

interact with creatine kinase (Fei et al. 2012; Balasubramaniam et al. 2015). Creatine kinases play a critical role in the buffering of ATP/ADP ratios in excitable cells such as in cardiomyocytes and neural cells, and as such are crucial for cellular homeostasis in the vertebrate heart and brain (Wang et al. 2011; Bush et al. 2011).

Based on a crystal structure of the ASB9/Elongin B, C (Figure 1), an initial model was proposed for the interaction of ASB9 with a dimer of creatine kinase (CK) (Muniz et al. 2013). Our group then used an array of solution biophysical studies to obtain experimental evidence of where CK docks on ASB9 and presented a revised model that aligned with our experimental data (Balasubramaniam et al. 2015). Enzymatic assays indicated that the ASB9-CK interaction retained half-the-sites reactivity, and our second-generation model therefore had the intrinsically disordered N-terminus of ASB9 occluding the active site of one CK monomer. Isothermal titration calorimetry (ITC) and surface plasmon resonance (SPR) data revealed that the ankyrin repeat domain of ASB9 binds to CK with nM affinity, and revealed that the N-terminal disordered residues contribute to even tighter affinity (Balasubramaniam et al. 2015). Hydrogen-deuterium exchange mass spectrometry (HDXMS) showed that when ASB9 binds CK residues 182-203 are protected (Balasubramaniam et al. 2015). The second-generation model captured these biophysical results including the interaction of the N-terminal repeats of ASB9 with the HDX protected residues in one of the CK monomers.

Here, we use small angle X-ray scattering (SAXS), isothermal titration calorimetry (ITC), pull-down assays, computational modeling and simulation to create and validate a third generation model of the ASB9-CK interaction that not only captures the interaction interface, but also the overall shape of the complex. We disrupt binding of ASB9 with CK through mutations of residues predicted to be in the binding interface by the model. Finally, we use this model to provide a description of the dynamic motions of ECS-type E3 ligase complexes that enables ubiquitin transfer to the target protein. Our results are, to our knowledge, the first to report an atomic-level mechanism that permits ubiquitin transfer in CRLs, which are the largest family of E3 ligases, ubiquitinate almost 20% of proteins degraded through the ubiquitin-mediate degradative pathway, and are an attractive therapeutic target in cancer (Zhao & Sun 2013).

Results and Discussion

Isothermal titration calorimetry refines which regions of the N-terminal disordered segment contribute to binding

Our second-generation model predicted that residues 1-18 were not in contact with CK whereas residues 19-35 of the disordered N-terminus of ASB9 lay in one active site of CK. To test whether this prediction was correct, we performed ITC experiments, titrating CK into a truncated mutant of ASB9 that only contains residues predicted to be in the complex interface from the docked poses, ASB9(19-252). Although the *c* value was too high to measure the K_d, the ΔH of the interaction was large, −19.2 kcal/mol, and could be determined with a high degree of precision (Figure 2A). This enthalpic contribution fully accounted for the CK interaction with ASB9, suggesting that residues 1-19, do not interact with CK in the binding interface.

Third generation docked model of the ASB9-CK complex

Based on our ITC results, the ASB9 structure (pdb 3D9H) was modified to include structures of the intrinsically disordered residues 19-35 which were not present in the crystal structure. Structures of ASB9(19-35) were generated with molecular dynamics (MD) simulations and these trajectories showed that this region sampled elongated structures similar to what was observed for the intrinsically disordered N-terminal 35 residues of ASB9 as we have previously reported (Balasubramaniam et al. 2015).

The crystal structure of CK (pdb 3B6R) has one monomer of the dimer in an open conformation and one in a closed conformation. As previously described in the second generation docking, we generated an open-open dimer from the crystal structure coordinates (Balasubramaniam et al. 2015). Based on the ITC results presented here, our current docked model starting from further minimized and equilibrated structures of the ASB9 (19-252) and of CK (open/open dimer).

Using the ZDOCK 3.0.2 server (Pierce et al. 2014), we obtained the top ten best docked poses (Table S1). The top scoring model, which we refer to as ZDOCK-1, had a score of 1778 and the second highest scoring model, ZDOCK-2, had a score of 1425 indicating a strong discrimination between the models. However all of the 10 poses appeared very similar in the orientation of the ASB9 ARD with respect to the CK active site (Figure 2B).

Analysis of ASB9-CK complex scattering profiles

We collected SAXS data for both ASB9(19-252)-CK and ASB9(1-252)-CK and both yielded scattering profiles with monotonically decaying scattering as a function of the scattering vector q and calculated R_g of 33.1 Å and 32.4 Å respectively (Figure 3A). We used the Debye formula for spherical scatters (Schneidman-Duhovny et al. 2011; Schneidman-Duhovny et al. 2013) to compute the SAXS profile from the ZDOCK-1 and ZDOCK-2 poses. The profile calculated from the ZDOCK-1 pose agreed with both the ASB9(19-252)-CK and the ASB9(1-252)-CK complexes, with χ^2 of 1.79 and 1.21, and R_g of 31.84 Å and 32.38 Å respectively. The profile calculated from the ZDOCK-2 pose showed poor agreement with the ASB9(19-252)-CK complex having a χ^2 of 7.34 and Rg of 31.90 but agreed with the ASB9(1-252)-CK complex, with χ^2 of 1.21 and R_g of 32.15 Å. Other protein-protein docking servers, such as RosettaDock (Lyskov & Gray 2008), FOXSDock (Schneidman-Duhovny et al. 2011), and ClusPro2.0 (Kozakov et al. 2013; Comeau et al. 2004) were also used and attained poses similar to the ZDOCK-1 and ZDOCK-2 poses, but agreement as assessed by χ^2 was not as good as for the ZDOCK-1 pose (Figure S1, Tables S1-S4). We chose to further explore the ZDOCK-1, which agreed best with the ASB9(19-252)-CK complex and the ZDOCK-2 pose, which agreed best with the ASB9(1-252)-CK complexes. Because the ZDOCK-1 pose agreed better with the SAXS profiles than poses from other docking servers, these were not pursued further.

The ZDOCK-1 and ZDOCK-2 poses appeared highly similar, with both poses showing the intrinsically disordered residues 22-35 interacting with one open active site in CK. However, the strong variation in χ^2 agreement with the SAXS data for the ASB9(19-252)-CK complex suggested significant differences. Indeed, when further analyzed, the total buried surface

area in the ZDOCK-1 structure was 3,970 Å^2, whereas only 2901 Å^2 was buried in the ZDOCK-2 pose. The buried surface area in the ZDOCK-1 pose also involved many more interacting side chains including ASB9 residues D36, W37, E42, I45, and H46 of ank1 and L78 of ank2 which interact with the active site loop of the occluded CK monomer. Residues S35 and P39 interact with the HDX-protected residues of that same CK monomer while residues H48, Q49, L50, N54, L55, and Q59 of ank1 and H81 and S83 of ank2 interact with the HDX-protected residues of the open CK monomer. Additionally, ASB9 residues A67, D68, H69, A100, D101 W102, E131, D133, L134, I164, S165 and H166 interact with active site loops of the occluded CK monomer (Figure 4A). The large amount of buried surface area is consistent with the very tight binding interaction (Balasubramaniam et al. 2015; Chothia & Janin 1975; Chakravarty et al. 2013). In the ZDOCK-2 pose, only residues W37 and W60 of ASB9 ank 1 interact with HDX-protected residues of the occluded CK active site. Additionally, residues H69, V98, T99, W102, E131, L134, D133, I164, S165, and H166 interact with the CK active site loops (Figure 4B).

ZDOCK-1 and ZDOCK-2 poses converge to similar binding interface in MD simulations

To test the stability and understand the structural dynamics of the ASB9-CK complex, we performed all-atom molecular dynamics (MD) simulations initiated from the atomic structures of the ZDOCK-1 and ZDOCK-2 poses. We simulated ASB9(22-252) and not ASB9(19-252), because in both the ZDOCK-1 and ZDOCK-2 poses, ASB9 residue R22 is the last N-terminal residue to lie within the CK open cleft, and we wished to avoid issues with force fields in oversampling collapsed structures of intrinsically disordered proteins (Henriques et al. 2015). Simulations were performed in triplicate for both the ZDOCK-1 and ZDOCK-2 poses.

Within tens of nanoseconds, the structures from the ZDOCK-2 simulations relaxed to an ASB9-CK interface that mimicked the ZDOCK-1 pose, while the interface of the ZDOCK-1 pose was maintained for over 300 ns of simulation (Figure 5, Movie 1). The relaxation of the ZDOCK-2 structures was measured with all-atom RMSD of the most critical interface residues from ASB9 (see below, residues D32, W36, I45, L50, I75, W102) and internal distances between residues implicated in the complex interface in the ZDOCK-1 pose (Figure 5A, Movie 1 and Fig S1). The internal distance between ASB9 residues I45 and L78 and CK active site loop residues P67 and Y68 relaxes to and is maintained at between 4-6 Å in all three parallel simulations from the ASB9(22-252)-CK complex (Figure 5A). A similar relaxation occurs for the internal distances between the center of mass of ank1 and CK residue V198, which is a residue in one of the HDXMS protected peptides (Movie 1, Fig S1).

Simulations provide new insight into the dynamics of CK that explain the protection of CK residues A182 to F192 (peptide 1 from HDXMS) and residues L193 to L203 (peptide 2 from HDXMS) in the helix-coil-helix region, located in front of the substrate-binding pocket, when in complex with ASB9. In the ZDOCK1 pose, ank1 of ASB9 binds directly to peptide 2 in both CK monomers. However, ASB9 does not bind directly to the CK peptide 1 in either CK monomer. Our simulations demonstrate that nanosecond motions lead to helix cracking causing exposure of residues E183 to L187 to exchange. This cracking is

significantly dampened when ASB9 is bound to CK, and likely accounts for the protection of these residues previously reported with HDXMS (Balasubramaniam et al. 2015).

Residues critical to the ASB9-CK interaction verified with mutagenesis

Structures from the ZDOCK1 simulation were clustered based on backbone RMSD (Figure 6A), and the cluster centroids were analyzed with the Robetta Alanine Scan server (Kortemme et al. 2002; Kortemme & Baker 2004) to predict the contributions of individual residues to the binding free energy of the ASB9-CK complex (Figure 6B). Residues that were previously found to be important in the ASB9-CK interaction, including D32, I45, and L78, were predicted to have a high ΔΔG between the alanine mutant and wild-type residue. Additionally, residues W37, L50, and W102 were also predicted to have a high ΔΔG and are highly conserved amongst ASB9 variants. Pull-down assays on these mutants revealed that, indeed residues W37, I45, L50, L78 and W102 are critical to the interaction of ASB9 with CK (Figure 6C). Thus, theoretical alanine scanning (Kortemme & Baker 2002; Kortemme et al. 2004) of the MD ensemble of ASB9-CK accurately predicted the key and necessary residues in the binding interface of the ASB9-CK complex.

Mechanism of ubiquitin-transfer to CK

With our experimentally validated model for the ASB9-CK complex, we constructed a complete model of the CK-targeting ECS-type E3 ligase, to uncover the conformational change necessary for ubiquitin transfer to CK. The E3 ligase model containing full-length ASB9, Elongins B and C, Cullin 5, Nedd8, Rbx1, E2, and ubiquitin but without the CK substrate was built as previously described (Muniz et al. 2013). The CK dimer was then added to this model based on our validated ZDOCK1 pose. To model the distance between the active thioester bond of E2-ubiquitin and lysines on CK, the ankyrin repeat domain of ASB9 from the E3 ligase model was aligned with the ankyrin repeat domain of ASB9 from the ZDOCK1 model. A distance of 82 Å was measured between the active thioester bond and the closest lysine on CK (Figure 7A).

The large distance between ubiquitin and CK in our E3 ligase model suggests the need for a large conformational change in the transfer of ubiquitin, and we found that calculating the theoretical motions of this E3 ligase model based on the structure alone provided incredible insight. We performed elastic network model analysis of our E3 ligase model to decipher if any slow motions of this multi-domain protein complex could be predicted (Zheng & Doniach 2003). Indeed, the slowest and most dominant normal mode observed in our E3 ligase model involves the coordinated folding of the Rbx1 linker domain with the bending of Cullin 5, and to a lesser extent Elongin C and ankyrin repeats 4-6 of ASB9 (Fig S2, S3), bringing the active thioester of E2-ubiquitin within 5.2 Å of the nearest lysine in CK (Figure 7B).

Remarkably, the dominant normal modes which bring the ubiquitin close to its CK substrate were not observed in elastic network models of the CK-E3 ligase models constructed with the ZDOCK-2 structure. Instead, the normal mode that achieved any proximity was a twisting motion, however the ubiquitin and CK remained over 50Å apart (Figure 7C). In addition, models that did not include the substrate, CK, were also incapable of motions that

brought the ubiquitin close to ASB9. Thus, not only did our latest model fit with all of the experimental data, it was the only one that moved in a manner consistent with the function of the entire E3 ligase, ubiquitin transfer. To our knowledge, this is the first reported model that suggests how CRLs transfer ubiquitin over 60 Å. Our model strongly suggests that correct substrate docking is required to initiate the large-scale motions necessary for ubiquitin transfer in ASB-containing E3 ligases.

Materials and methods

Materials and methods used in this study for mutagenesis, protein purification, isothermal titration calorimetry, creatine kinase assay, and protein docking were previously reported (Balasubramaniam et al. 2015). Here, the same method was used for performing protein docking experiments as previously reported, except that the starting structures of ASB9(1-252) and CK(open/open) were minimized and equilibrated to sample more favorable side-chain and hydrogen-bond orientations with Maestro (Schrodinger Release 2015-4).

Small Angle X-ray Scattering

Proteins were purified as previously described (Balasubramaniam et al. 2015), concentrated to 2 mg/mL for ASB9(1-252)-CK complex, and 3 mg/mL for the ASB9(19-252)-CK complex, and sent out to the SIBYLS Beamline for analysis.

Molecular Dynamics Simulations

Three parallel ASB9(1-252)-CK (CK in complex with ASB9) and ASB9(22-252)-CK simulations starting from the ZDOCK-1 and ZDOCK-2 poses were performed using the AMBER ff99SB force field (Hornak 2006) in TIP3P (Jorgensen et al. 1983) water box. The orthorhombic water-box around the hetero-trimer was built with dimensions listed below in Table 1, with periodic boundary conditions were prepared in maestro (Schrodinger Release 2015-4). The N-termini and C-termini were capped with acetyl and methyl groups respectively. The total system included a low (0.15 M) concentration of sodium chloride in water and 36 Na^+ to neutralize. The protonation states of the system at pH 7.0 was performed with PROPKA (Li et al. 2005). Simulations were performed with NVIDIA GK110 (GeForce GTX Titan) GPU using the CUDA version of PMEMD in AMBER12 (Hornak 2006; Case et al. 2005). The simulations were relaxed using 119,000 steps of energy minimization. For 3000 steps, only hydrogens were minimized with 100.0 kcal/$Å^2$xmol of restraint, 500 steps of steepest descent algorithm-based minimization and 2500 steps of conjugate-gradient algorithm-based minimization. Following, all hydrogens and waters were minimized in 6000 steps. All waters, hydrogens and protein side chains were minimized during the next 40,000 steps of minimization. The last 70,000 steps of minimization, all atoms were minimized. Following minimization, the system was heated to 303.15K in 4000 steps with a 4.0 kcal/$Å^2$xmol restraint on the protein backbone atoms. Three equilibration steps were then performed, each totaling 250 ps of simulation in which all of the backbone atoms except ASB9(1-35) were restrained with 3.0 kcal/$Å^2$xmol, 2.0 kcal/$Å^2$xmol, and finally 1.0 kcal/$Å^2$xmol of force. Long-range electrostatics were

calculated using particle mesh Ewald (PME) method (Case et al. 2005), with a 10 Å cutoff and a 1.2 Å grid spacing.

Three simulations initiated from the CK homodimer (PDB 3DRB), and five simulations initiated from maestro (Schrodinger Release 2015-4) built ASB9 (19-35) were performed with the same force field, water model, salt concentration, and simulation conditions as described for the ASB9-CK simulations above. The net charge of the solute was counter-balanced with the addition of 30 Na^+ ions for the CK homo-dimer and no counterbalance was needed for the ASB9 (19-35) system. The orthorhombic boundary conditions for CK homodimer were 89.57 Å × 87.0 Å × 117.2 Å, with a total of 86,108 atoms in the system. The cubic boundary conditions for ASB9 (19-35) were 73.4 × 73.5 × 73.4 Å per side, with a total of 32,623 atoms in the system. The CK homo-dimer structure was taken from the pdb 3DRB (Bong et al. 2008). The ligands were removed from the structure since all of the experiments were performed on apo CK homo-dimer. Residues 1-5 were not resolved in the crystal structure and were not built into the CK homo-dimer since the location of these residues varies among CK analogs (Lahiri et al. 2002; Rao et al. 1998; Shen et al. 2001; Tisi et al. 2001) and important for interactions with other proteins but not for CK's interaction with ASB9.

Molecular Dynamics Analysis

Backbone RMSD-based conformational clustering was performed using the gromos algorithm (Daura et al. 1999) with GROMACS 4.0.5 (Hess 2008) software. For the ASB9-CK systems, atomic coordinates were extracted at every 6 ps and aligned to the backbone atoms of the CK monomer with ASB9's D32 docked into its active site. Various RMSD cutoffs for the entire backbone (1.25 Å, 1.55 Å, 1.7 Å, 2.1 Å) and 2.1 Å for consistency as this produced the best clustering for the 25 ns simulations. After calculating the RMSD distance matrix, the gromos algorithm clusters the structures and determines the cluster centroid as previously described (Demir et al. 2011).

The number of hydrogen bonds formed between each residue's backbone amide and oxygen water in the simulation was performed through the use of in-house python scripts and cpptraj (Roe & Cheatham III 2013). The standard cpptraj settings for angle and distance definitions for a hydrogen bond were used. Each frame of the trajectory was considered and the total number of hydrogen bond contacts was tallied and reported as a percentage of the total frames in the simulation.

Robetta analysis

Robetta analysis (Kim et al. 2004) was performed on each cluster centroid of the above described 2.1 Å RMSD-based clustering without specifying any mutation list.

Mutational analysis of Robetta results

CKB, cloned into a pET11a vector, and N-terminal His-tagged ASB9 (35-252) mutants, cloned into a pHis8 vector, were coexpresssed in *E. coli* BL21(DE3) cells. ASB9 mutants W37A, I45A, I45R, L50A, L78A, L78R and W102A were generated by site-directed mutagenesis from the ASB9 (35-252) construct. Cells were grown at 37° C to an OD of 0.7,

and induced with 0.4 mM isopropyl β-D-1-thiogalactopyranoside overnight at 18° C in 50 mL LB medium. The cell pellet was resuspended in 2 mL of buffer A (50mM Tris-HCl pH 8.0, 50mM NaCl, 20 mM imidazole, 1 mM DTT, 0.5 mM PMSF), sonicated on ice and centrifuged for 20 min at 4° C and 14,000 rpm. The supernatant was loaded onto a 1 mL HisTrap HP (GE Healthcare) column at 4° C equilibrated with buffer A, then washed with 2 mL of buffer A and eluted with 3 mL of buffer A supplemented with 500 mM imidazole. Then, 20 μL aliquots of each purification step (supernatant, SN; flow-through, FT; wash, W; elution, E) were analyzed by SDS-PAGE with 15% polyacrylamide gels.

Elastic Network Model

The CK Cullin-5 E3 Ubiquitin Ligase complex was built was previously described (Thomas et al. 2013), with the ASB9(19-252)-CK complex of the equilibrated ZDOCK-1 pose, the equilibrated ZDOCK-2 pose, and cluster centroids from both simulations. The various E3 Ligases were uploaded to the AD-ENM (Elastic Network Model) server (Zheng & Brooks 2005). For the output specification, 10 of the lowest modes were output, with amplitude of displacement per mode of 24, and 30 frames generated. For the parameters settings, a 0 Å distance for coarse-graining was chosen as well as a 15 Å distance cutoff for elastic interaction between CA atoms.

Supplementary Material

Refer to Web version on PubMed Central for supplementary material.

Acknowledgments

This work was funded in part by the Director's New Innovator Award Program NIH DP2 OD007237 and an NSF XSEDE award RAC CHE060073N to REA. Funding and support from the National Biomedical Computation Resource is provided through NIH P41 GM103426. JMS was supported by NIH Molecular Biophysics Training Grant T32 GM008326. Additional resources from the Keck II Computing and Visualization facility are gratefully acknowledged. REA is a co-founder of Actavalon, Inc.

References

Balasubramaniam D, et al. How the ankyrin and SOCS box protein, ASB9, binds to creatine kinase. Biochemistry. 2015; 54(8):1673–1680. Available at: http://pubs.acs.org/doi/abs/10.1021/bi501420n. [PubMed: 25654263]

Bong SM, et al. Structural studies of human brain-type creatine kinase complexed with the ADP-Mg2+-NO3--creatine transition-state analogue complex. FEBS Letters. 2008; 582(28):3959–3965. Available at: http://dx.doi.org/10.1016/j.febslet.2008.10.039. [PubMed: 18977227]

Bush DJ, et al. The structure of lombricine kinase: Implications for phosphagen kinase conformational changes. Journal of Biological Chemistry. 2011; 286(11):9338–9350. [PubMed: 21212263]

Case DA, et al. The Amber biomolecular simulation programs. Journal of Computational Chemistry. 2005; 26(16):1668–1688. [PubMed: 16200636]

Chakravarty D, Guharoy M, Robert CH. Reassessing buried surface areas in protein –protein complexes. 2013; 22:1453–1457.

Chothia C, Janin J. Principles of protein-protein recognition. Nature. 1975; 256:705–708. [PubMed: 1153006]

Comeau SR, et al. ClusPro: A fully automated algorithm for protein-protein docking. Nucleic Acids Research. 2004; 32(WEB SERVER ISS.):96–99.

Daura X, et al. Peptide Folding: When Simulation Meets Experiment. Angewandte Chemie International Edition. 1999; 38:236–240. Available at: http://doi.wiley.com/10.1002/(SICI)1521-3773(19990115)38:1/2<236::AID ANIE236>3.0.CO;2-M.

Debrincat MA, et al. Ankyrin repeat and suppressors of cytokine signaling box protein Asb-9 targets creatine kinase B for degradation. Journal of Biological Chemistry. 2007; 282(7):4728–4737. [PubMed: 17148442]

Demir Ö, et al. Ensemble-based computational approach discriminates functional activity of p53 cancer and rescue mutants. PLoS Computational Biology. 2011; 7(10)

Deshaies R, Joazeiro C. RING Domain E3 Ubiquitin Ligases. Annual Reviews in Biochemistry. 2009; 78

Duda DM, et al. Structural Insights into NEDD8 Activation of Cullin-RING Ligases: Conformational Control of Conjugation. Cell. 2008; 134(6):995–1006. [PubMed: 18805092]

Fei X, et al. Crystal structure of Human ASB9-2 and substrate-recognition of CKB. Protein Journal. 2012; 31(4):275–284. [PubMed: 22418839]

Henriques J, Cragnell C, Skepo M. Molecular Dynamics Simulations of Intrinsically Disordered Proteins: Force Field Evaluation and Comparison with Experiment. Journal of Chemical Theory and Computation. 2015; 11(7):3420–3431. [PubMed: 26575776]

Hess B. Kutzner C. GROMACS 4: algorithms for highly efficient, load-balanced, and scalable molecular simulation. 2008:435–447.

Hornak V. Abel R. Comparison of Multiple Amber Force Fields and Development of Improved Protein Backbone Parameters. 2006:572–581.

Jorgensen WL, et al. Comparison of simple potential functions for simulating liquid water. The Journal of Chemical Physics. 1983; 79(2):926. Available at: http://scitation.aip.org/content/aip/journal/jcp/79/2/10.1063/1.445869\nhttp://link.aip.org/link/?JCPSA6/79/926/1.

Kerscher O, Felberbaum R, Hochstrasser M. Modification of proteins by ubiquitin and ubiquitin-like proteins. Annual Review of Cellular and Developmental Biology. 2006; 22:159–180.

Kim DE, Chivian D, Baker D. Protein structure prediction and analysis using the Robetta server. Nucleic Acids Research. 2004; 32(WEB SERVER ISS.):526–531.

Kohroki J, et al. ASB proteins interact with Cullin5 and Rbx2 to form E3 ubiquitin ligase complexes. FEBS Letters. 2005; 579(30):6796–6802. Available at: http://linkinghub.elsevier.com/retrieve/pii/S0014579305013761. [PubMed: 16325183]

Kortemme T, Baker D. A simple physical model for binding energy hot spots in protein-protein complexes. Proceedings of the National Academy of Sciences of the United States of America. 2002; 99(22):14116–14121. [PubMed: 12381794]

Kortemme T, Kim DE, Baker D. Computational alanine scanning of protein-protein interfaces. Science's STKE : signal transduction knowledge environment. 2004; 2004(219):pl2. Available at: http://www.ncbi.nlm.nih.gov/pubmed/14872095. [PubMed: 14872095]

Kozakov D, et al. How good is automated protein docking? Proteins: Structure, Function and Bioinformatics. 2013; 81(12):2159–2166.

Kwon S, et al. ASB9 interacts with ubiquitous mitochondrial creatine kinase and inhibits mitochondrial function. BMC biology. 2010; 8(March):23. [PubMed: 20302626]

Lahiri SD, et al. The 2 .1 Å Structure of Torpedo californica Creatine Kinase Complexed with the ADP-Mg2+-NO3 --Creatine Transition-State Analogue Complex. 2002; (3):13861–13867.

Li H, Robertson AD, Jensen JH. Very fast empirical prediction and rationalization of protein pK a values. Proteins: Structure, Function and Genetics. 2005; 61(4):704–721.

Lyskov S, Gray JJ. The RosettaDock server for local protein-protein docking. Nucleic acids research. 2008; 36(Web Server issue):233–238.

Muniz JR, et al. Molecular architecture of the ankyrin SOCS box family of Cul5-dependent E3 ubiquitin ligases. J Mol Biol. 2013; 425:3166–3177. [PubMed: 23806657]

Petroski MD, Deshaies RJ. Function and regulation of cullin-RING ubiquitin ligases. Nat Rev Mol Cell Biol. 2005; 6:9–20. [PubMed: 15688063]

Pierce BG, et al. ZDOCK server: Interactive docking prediction of protein-protein complexes and symmetric multimers. Bioinformatics. 2014; 30(12):1771–1773. [PubMed: 24532726]

Rao JK, Bujacz G, Wlodawer A. Crystal structure of rabbit muscle creatine kinase. FEBS letters. 1998; 439(1-2):133–137. Available at: http://www.ncbi.nlm.nih.gov/pubmed/9849893. [PubMed: 9849893]

Roe DR, Cheatham III TE. PTRAJ and CPPTRAJ: software for processing and analysis of molecular synamics trajectory data. Journal of Chemical Theory and Computation. 2013; 9(7):3084–3095. Available at: http://www.chemeurope.com/en/publications/580240/ptraj-and-cpptraj-software-for-processing-and-analysis-of-molecular-dynamics-trajectory-data.html. [PubMed: 26583988]

Schneidman-Duhovny D, et al. Accurate SAXS profile computation and its assessment by contrast variation experiments. Biophysical Journal. 2013; 105(4):962–974. Available at: http://dx.doi.org/10.1016/j.bpj.2013.07.020. [PubMed: 23972848]

Schneidman-Duhovny D, Hammel M, Sali A. Macromolecular docking restrained by a small angle X-ray scattering profile. Journal of Structural Biology. 2011; 173(3):461–471. Available at: http://dx.doi.org/10.1016/j.jsb.2010.09.023. [PubMed: 20920583]

Shen YQ, et al. Structure of human muscle creatine kinase. Acta crystallographica. Section D, Biological crystallography. 2001; 57(Pt 8):1196–1200. [PubMed: 11517911]

Thomas JC, et al. Multimeric complexes among ankyrin-repeat and SOCS-box protein 9 (ASB9), ElonginBC, and cullin 5: Insights into the structure and assembly of ECS-type Cullin-RING E3 ubiquitin ligases. Biochemistry. 2013; 52(31):5236–5246. [PubMed: 23837592]

Tisi D, Bax B, Loew A. The three-dimensional structure of cytosolic bovine retinal creatine kinase. Acta Crystallographica Section D: Biological Crystallography. 2001; 57(2):187–193. [PubMed: 11173463]

Wang Y, et al. Dissimilarity in the folding of human cytosolic creatine kinase isoenzymes. PLoS ONE. 2011; 6(9):28–34.

Zhao Y, Sun Y. Cullin-RING Ligases as attractive anti-cancer targets. Current pharmaceutical design. 2013; 19(18):3215–25. Available at: http://www.pubmedcentral.nih.gov/articlerender.fcgi?artid=4034125&tool=pmcentrez&rendertype=abstract. [PubMed: 23151137]

Zheng W, Brooks BR. Normal modes based prediction of protein conformational changes guided by distance constraints. Biophysical Journal. 2005; 88:3109–3117. [PubMed: 15722427]

Zheng W, Doniach S. A comparative study of motor-protein motions by using a simple elastic-network model. Proceedings of the National Academy of Sciences of the United States of America. 2003; 100(23):13253–13258. [PubMed: 14585932]

- Protein-protein docked models of ASB9-CK align with new ITC and SAXS data.
- Simulations from these models converge to a similar complex interface.
- Key residues in this interface are validated with mutagenesis and pull-down assays.
- A dominant mode of motion of the CK-targeting E3 ligase is revealed.

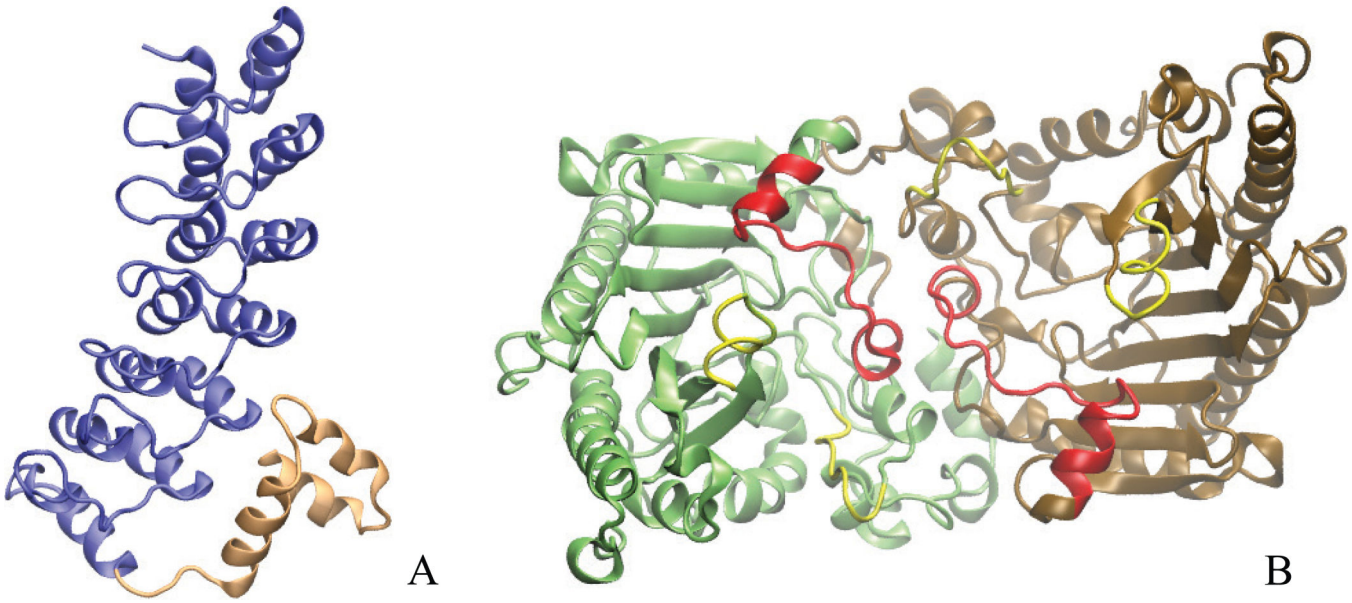

Figure 1.
Structures of (A) the ankyrin repeat and SOCS box protein 9 (ASB9, PDB 3ZKJ) and (B) the creatine kinase homo-dimer made up of two open monomers (PDB 3DRB).

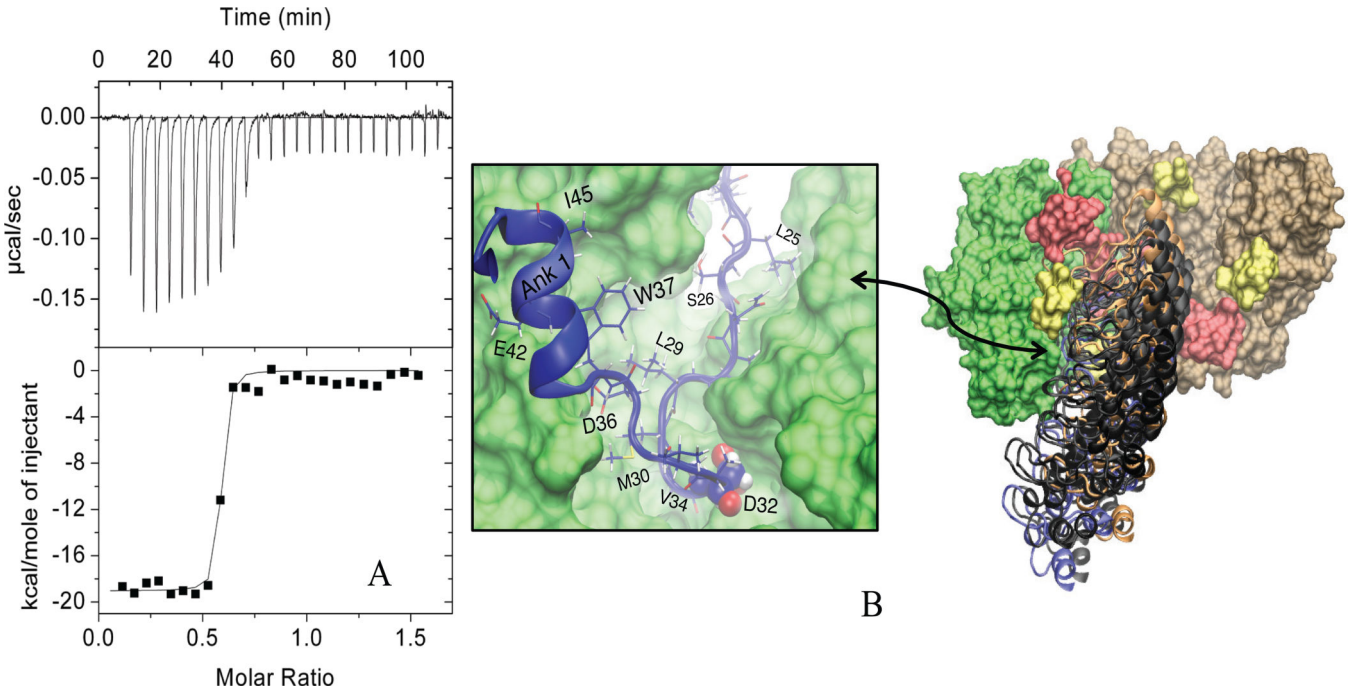

Figure 2. N-terminal residues of ASB9 form half of the binding interface between ASB9 and CK

(A) ITC thermogram and fit for 37 µM CK (dimer concentration) (in syringe) binding to 5 µM ASB9(19-252) (in cell). (B) Residues of the intrinsically disordered N-terminus of ASB9 (blue) loop through the active site of CK (green) in our third generation docked model. (C) Overlay of 6 of our best docked models from the third generation docking. ZDOCK1 (blue) and ZDOCK2 (orange) poses of ASB9 are shown for reference. CK dimer (green/brown) is depicted in a surface model, with active site loops (yellow) and HDXMS protected residues (red) similarly depicted.

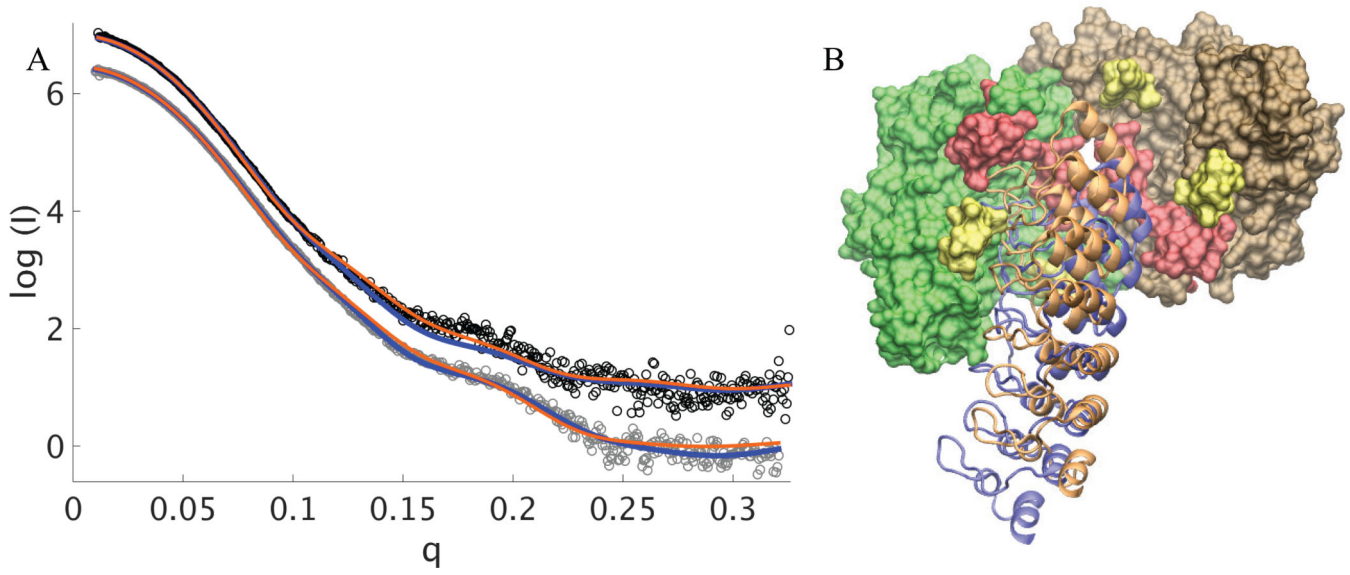

Figure 3. Docked structures align with SAXS profiles for the ASB9(1-252) complex with CK and for the ASB9(19-252) complex with CK

(A) SAXS profiles for ASB9(1-252)-CK complex (black) and for ASB9(19-252)-CK complex (grey) are shown as scatter plot. Theoretical scattering profiles for the ZDOCK1 pose, with or without residues 1-18, are shown in blue. Theoretical scattering profiles for the ZDOCK2 pose, with or without residues 1-18, are shown in orange. (B) Relative orientation of the ankyrin repeat domain of ASB9 in the ZDOCK1 (blue) or ZDOCK2 (orange) pose respectively. HDXMS protected residues (red) and active site loops (yellow) of CK are shown for reference.

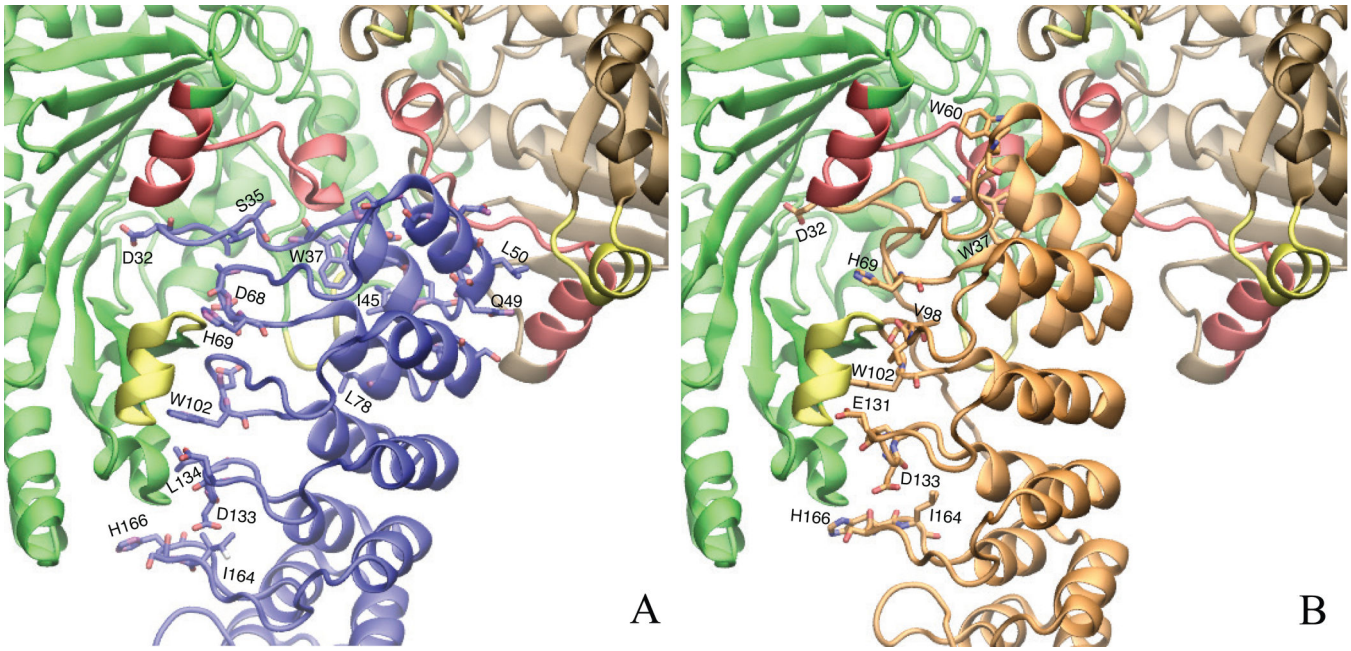

Figure 4. Residues from ASB9 involved in the binding interface for the third generation model

(A) Residues from ASB9 in the ZDOCK1 pose include D32, S35, W37, I45, Q49, L50, D68, H69, L78, W102, D133, L134, I164, and H166. (B) Residues for ASB9 in the ZDOCK2 pose include D32, W37, W60, H69, V98, W102, E131, D133, I164, and H166..

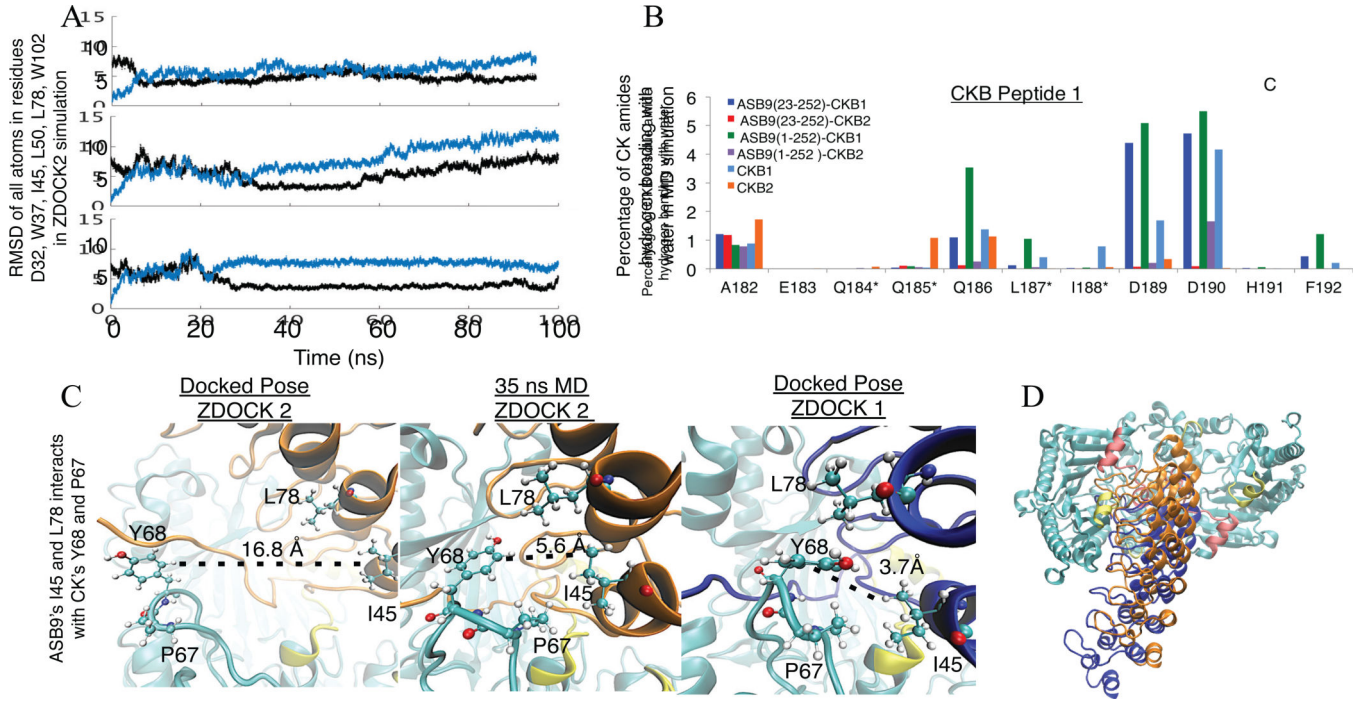

Figure 5. Simulations from the best docked poses (ZDOCK1, ZDOCK2) converge to a similar binding interface and provide an explanation for HDX protection of CK residues by ASB9

(A) Root Mean Squared Distance (RMSD) of all atoms in residues in the ZDOCK1 interface, W37, I45, L50, L78, and W102, measured over three separate MD trajectories starting from the ZDOCK2 pose. Within a few ns, the RMSDs all decrease to <5 Å in all three simulations, and are maintained under 5 Å in two of the three simulations. (B) Percentages of amide hydrogen bonding with water is reported for residues of peptide 1 in CK from simulation of ASB9(1-252) in complex with CK, simulations of ASB9(22-252) in complex with CK, and simulations of CK alone in solution. (C) Figures showing the initial and final distances between ASB9 and CK residues in the ZDOCK2 simulation compared to the distance of the ZDOCK1 pose. This interface eventually converges to a very similar interface. (D) For reference, the structures of the ZDOCK1 pose and ZDOCK2 pose.

A

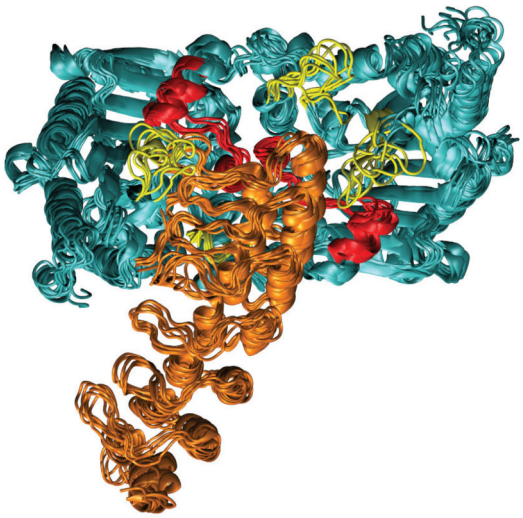

B

ASB9 residue	Average ΔΔG	Sequence Conserve	Sequence Variety
D32	1.61 ± 0.25	15/18	G
V34	1.11 ± 0.14	16/18	E
D36	2.59 ± 0.84	16/18	Y
W37	1.17 ± 0.24	17/18	-
I45	0.70 ± 0.10	14/18	L, V
Q49	1.78 ± 0.68	1/18	L, V
L50	1.46 ± 0.12	18/18	-
L78	0.70 ± 0.37	18/18	-
W102	1.43 ± 0.86	17/18	R

C

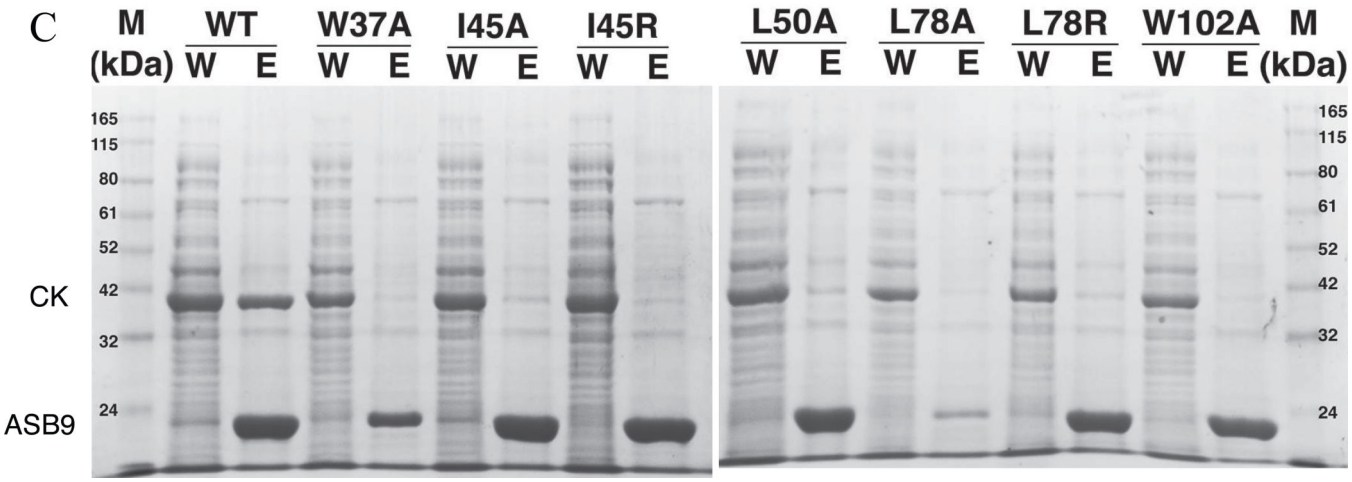

Figure 6. MD simulations reveal which residues are most important in the binding interface and show mobility of active site residues

(A) Cluster centroids of the ASB9(22-252)-CK simulations. (B) Robetta alanine scan results reported as an average over all cluster centroids. (B) Pull-down assays of indicated alanaine mutants reveals that CK is not pull down sufficiently by any of these mutants.

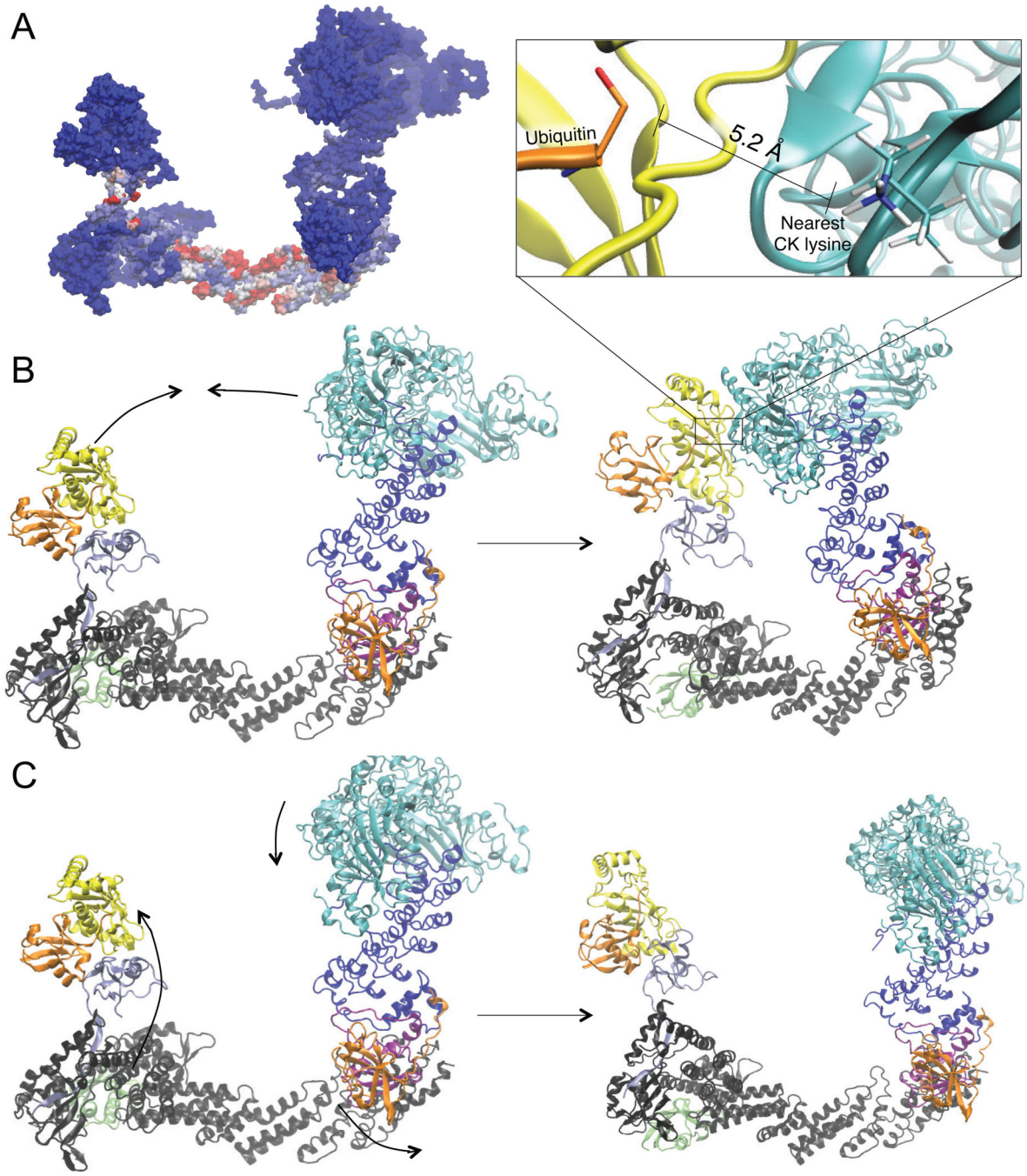

Figure 7. The CK-targeting ECS-type E3 ligase motion revealed by elastic network model

(A) Surface representation of E3 ligase colored based on the mobility of residues in elastic network model. (B) Lowest-frequency normal mode of E3 ligase model, built with the ZDOCK-1 pose for the ASB9-CK complex, brings active thioester of E2-ubiquitin within 5.2 Å of a CK lysine. (C) Normal mode of E3 ligase model, built with the ZDOCK-2 pose for the ASB9-CK complex, brings the active thioester of E2-ubiquitin closest to a CK lysine, within ~ 50 Å.

	ASB9(1-252)-CK ZDOCK1	**ASB9(1-252)-CK ZDOCK2**	**ASB9(23-252)-CK ZDOCK1**	**ASB9(23-252)-CK ZDOCK2**
Box Dimensions	123.73 Å × 99.8 Å × 125.96 Å	119.7 Å × 128.4 Å × 97.2 Å	129.35 Å × 97.6 Å × 91.2 Å	88.5 Å × 126.3 Å × 108.8 Å
Total Atoms	131,749	125,446	96,116	102,915
Neutralizing salt	37 Na^+	36 Na^+	38 Na^+	37 Na^+